Evidence for a Surface Confined Ion-to-Electron Transduction Reaction in Solid-Contact Ion-Selective Electrodes Based on Poly(3-octylthiophene)

ARTICLE *in* ANALYTICAL CHEMISTRY · SEPTEMBER 2013

Impact Factor: 5.64 · DOI: 10.1021/ac4024999 · Source: PubMed

11 AUTHORS, INCLUDING:

Ewa Grygolowicz-Pawlak

Nanyang Technological University

23 PUBLICATIONS **295** CITATIONS

SEE PROFILE

Michael James

Australian Synchrotron

148 PUBLICATIONS **2,236** CITATIONS

SEE PROFILE

Eric Bakker

University of Geneva

291 PUBLICATIONS **13,795** CITATIONS

SEE PROFILE

analytical chemistry

Article

pubs.acs.org/ac

Evidence for a Surface Confined Ion-to-Electron Transduction Reaction in Solid-Contact Ion-Selective Electrodes Based on Poly(3-octylthiophene)

Jean-Pierre Veder,[†,#] Roland De Marco,[*,†,§] Kunal Patel,[†] Pengchao Si,[†] Ewa Grygolowicz-Pawlak,[†,‡] Michael James,[⊥,¶] Muhammad Tanzirul Alam,[§] Manzar Sohail,[§] Junqiao Lee,[†] Ernö Pretsch,[∥] and Eric Bakker[†,‡]

[†]Department of Chemistry, Curtin University, GPO Box U1987, Perth, Western Australia 6109, Australia

[#]CSIRO Process Science and Engineering, Box 312, Clayton South, Melbourne, Victoria 3169, Australia

[§]Faculty of Science, Health, Education and Engineering, University of the Sunshine Coast, 90 Sippy Downs Drive, Sunshine Coast, Queensland 4556, Australia

[‡]Department of Inorganic and Analytical Chemistry, University of Geneva, Quai Ernest-Ansermet 30, CH-1211 Geneva, Switzerland

[⊥]Bragg Institute, Australian Nuclear Science and Technology Organisation, Locked Bag 2001, Kirrawee DC, NSW 2232, Australia

[¶]Australian Synchrotron, 800 Blackburn Rd, Clayton, Melbourne, Victoria 3168, Australia

[∥]ETH Zürich, Institute of Biogeochemistry and Pollutant Dynamics (IBP), Universitätstrasse 16, CH-8092, Zürich, Switzerland

ABSTRACT: The ion-to-electron transduction reaction mechanism at the buried interface of the electrosynthesized poly(3-octylthiophene) (POT) solid-contact (SC) ion-selective electrode (ISE) polymeric membrane has been studied using synchrotron radiation-X-ray photoelectron spectroscopy (SR-XPS), near edge X-ray absorption fine structure (NEXAFS), and electrochemical impedance spectroscopy (EIS)/neutron reflectometry (NR). The tetrakis[3,5-bis(triflouromethyl)phenyl]borate ($TFPB^-$) membrane dopant in the polymer ISE was transferred from the polymeric membrane to the outer surface layer of the SC on oxidation of POT but did not migrate further into the oxidized POT SC. The $TFPB^-$ and oxidized POT species could only be detected at the outer surface layer (≤14 Å) of the SC material, even after oxidation of the electropolymerized POT SC for an hour at high anodic potential demonstrating that the ion-to-electron transduction reaction is a surface confined process. Accordingly, this study provides the first direct structural evidence of ion-to-electron transduction in the electropolymerized POT SC ISE by proving $TFPB^-$ transport from the polymeric ISE membrane to the oxidized POT SC at the buried interface of the SC ISE. It is inferred that the performance of the POT SC ISE is independent of the thickness of the POT SC but is instead contingent on the POT SC surface reactivity and/or electrical capacitance of the POT SC. In particular, the results suggest that the electropolymerized POT conducting polymer may spontaneously form a mixed surface/bulk oxidation state, which may explain the unusually high potential stability of the resulting ISE. It is anticipated that this new understanding of ion-to-electron transduction with electropolymerized POT SC ISEs will enable the development of new and improved devices with enhanced analytical performance attributes.

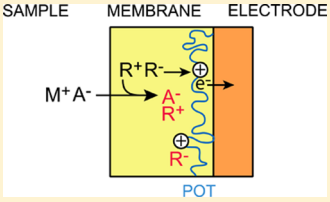

The emergence of coated-wire electrodes[1] (CWEs) in the early 1970s represented a significant advancement specifically with regard to ion-selective electrode (ISE) miniaturization, although these electrodes have generally lacked long-term potential stability.[2,3] This was later attributed to a poorly defined charge-transfer process at the interface between the ISE membrane and the electrically conductive substrate.[4] Furthermore, the gradual formation of a water layer at the buried interface of the ISE[5,6] also degraded the response attributes of the CWE ISE, which was a significant road block for the technological advancement of this important class of sensors. The use of solid-contacts (SCs) allowed the redox reaction of the SC to be coupled with ionic transference from the polymeric ISE membrane at the buried interface of the system, thereby providing a stabilized electrode,[7] which represented a major advancement in the field of SC ISEs.[8,9]

Since the development of SC sensors, they have generally comprised thick layers (i.e., several micrometers) of electroactive polymers, redox-active self-assembled monolayers[7,10−14] (SAMs), or carbonaceous materials with high surface capacitance[15−17] possessing both electronic and ionic conductivity, so as to support ion-to-electron transduction at the buried interface between the SC and ISE membrane. Poly(3-octylthiophene) (POT) has been shown to be a particularly attractive SC ISE possessing excellent potential stability, with this potential stability appearing to be counterintuitive. A fully oxidized or reduced POT layer should give rise to an undefined and unstable redox potential at the inner membrane side, while

Received: August 7, 2013
Accepted: September 30, 2013
Published: September 30, 2013

   dx.doi.org/10.1021/ac4024999 | *Anal. Chem.* 2013, 85, 10495−10502

a mixed potential (this term is explained at http://goldbook.iupac.org/M03944.html) is expected to change according to the membrane and sample composition and is also unable to explain this desired potentiometric stability. Recently, Kim and Amemiya[18] along with Si and Bakker[19] showed in separate but related studies that ion-to-electron transduction in a conducting polymer (CP) occurs via a 3-phase process, i.e., oxidation of the conducting polymer, and subsequent transfer of anion from the solution to the membrane and from the membrane to the conducting polymer, respectively. Oxidation of POT in the absence of lipophilic ion-exchanger is very difficult since it must instead be accompanied by extraction of a hydrophilic anion from the sample phase but can be promoted by a cation-exchanger in the membrane since a hydrophilic cation may be expelled from the membrane as POT is oxidized. Similar theories were adopted by Fibbioli et al.[12] and Crespo et al.[16] in explaining ion-to-electron transduction of redox active SAM and single wall carbon nanotube based ISEs, respectively. However, there has not been a rigorous surface study of the buried interface between the SC and ISE membrane to elucidate the ion-to-electron transduction reaction mechanism (e.g., surface confined or diffusion controlled reactivity), which is critical in terms of understanding the response and lowering the limit of detection of ISEs with enhanced selectivity, and this is the subject of the present paper.

The present study was focused on an electropolymerized POT SC ISE, with a view of elucidating the ion-to-electron transduction mechanism in this system. The POT SC was chosen since it yields a high and unexplained potential stability, does not appear to influence membrane selectivity, and can result in nanomolar detection limits because of its ability to avoid the formation of a deleterious water layer.[20] Consequently, one may study ion-to-electron transduction at the buried interface of POT/ISE membrane without the possibility of side reactions and/or interfering processes. Synchrotron radiation-X-ray photoelectron spectroscopy (SR-XPS), near edge X-ray absorption fine structure (NEXAFS), and electrochemical impedance spectroscopy/neutron reflectometry (EIS/NR) were used to probe the electrochemically driven ingression of the anion from the ISE membrane into the oxidized POT SC. SR-XPS, NEXAFS, and EIS/NR are powerful surface analysis tools that can ascertain the chemical and physical nature of the POT SC and follow any physical and chemical changes associated with oxidation of the POT SC. SR-XPS can provide rich information about surface chemical states controlling the behavior of the SC ISE, permitting structure elucidation of the outermost surface layers of the SC at elemental concentrations of ≈1 at %.[21] Also, due to the tunability of the SR beam, it is possible to attain lower detection limits in SR-XPS, where a beam energy as close as practicable to the absorption edge elevates the photoabsorption cross section and the concomitant detection limit of the probed core atomic orbital by several orders of magnitude. Likewise, NEXAFS is a powerful technique that can distinguish between the oxidized and neutral states of POT due to variations in the fine structure of the excited edge spectrum. This fine structure is associated with nearest atomic neighbors experiencing constructive and destructive scattering of electrons during photoionization of the core orbital of the atom. Furthermore, another asset of NEXAFS is its polarization dependence, which can be very sensitive to state symmetry and molecular orientation.[22] EIS/NR is a coupling of powerful characterization techniques that permits real-time and in situ investigation of the chemical and physical factors, influencing the behavior of the buried interface between the polymer ISE membrane and POT SC, and provides an in depth nanostructural perspective of the buried interface, so as to complement and validate the SR-XPS and NEXAFS data.

In this work, we have undertaken a rigorous study of the mechanism of ion-to-electron transduction in the POT SC ISE by using electrochemical and surface analysis techniques. This study provides the first direct and unequivocal structural evidence of ion-to-electron transduction in the electropolymerized POT SC ISE, as compared to inferred evidence in previous electrochemical studies. Surface analysis has identified reaction sites and elucidated the reaction mechanism by detecting the transference of ions and oxidation of POT at the buried interface between SC and ISE membrane, and this represents a major advancement in knowledge on the ion-to-electron transduction mechanism in the POT SC ISE.

EXPERIMENTAL SECTION

Materials. High molecular weight poly(vinylchloride) (PVC), *N*,*N*-dicyclohexyl-*N*′,*N*′-dioctadecyl-3-oxapentanediamide (calcium ionophore IV), potassium and sodium tetrakis [3,5-bis-(trifluoromethyl)phenyl]borate (KTFPB and NaTFPB), tridodecylmethylammonium chloride (TDMACl, 97%), and bis(2-ethylhexyl)-sebacate (DOS) were sourced as Selectophore Fluka reagents through Sigma-Aldrich (Castle Hill, New South Wales, Australia). Anhydrous lithium perchlorate (99.99%), 3-octylthiophene, regioregular POT (99.99%), anhydrous acetonitrile (99.8%), anhydrous *N*,*N*-dimethyl-formamide (DMF, 99.8%), and inhibitor-free tetrahydrofuran (THF, 99.8%) were also obtained from Sigma-Aldrich (Castle Hill, New South Wales, Australia). Analytical grade sulfuric acid and hydrogen peroxide used in piranha etching of silica wafers were sourced from the Ajax Chemical Co. (Taren Point, New South Wales, Australia). Laboratory grade xylene used in degreasing of silica wafers was obtained from Chem-Supply (Gillman, Port Adelaide, South Australia). The highly polished silicon wafers (8 cm × 4 cm × 2 cm) used in NR measurements (boron doped for electrical conductivity) were obtained from Crystran Ltd. (Dorset, United Kingdom). Gold (111) mirrors used in the SR-XPS and NEXAFS studies were sourced from ArrandeeTM (Werther, Germany). Milli-Q water was used to prepare all aqueous solutions unless otherwise specified.

Electrochemical Measurements. Electropolymerization of POT on 12 mm × 12 mm Au(111) and its subsequent oxidation were performed in a custom designed Teflon made three-electrode cell. In this cell configuration, Au(111) mirror, solid-state Ag/AgCl wire, and Pt coiled-wire served as the working, reference, and counter electrodes, respectively. Electropolymerization was carried out in a solution of 0.1 M 3-octylthiophene and 0.1 M $LiClO_4$ in acetonitrile by cycling potential (30 scans) in the range of 0 to 1.5 V vs Ag/AgCl at a scan rate of 0.1 V s^{-1}. Electrolytes were deoxygenated by purging with pure nitrogen for about 15 min, and a nitrogen flow was maintained over the liquids during polymerization. After electropolymerization, the POT film was discharged at 0 V for 5 min and subsequently washed with acetonitrile to remove residual amounts of electrolyte. Prior to use, POT SCs were allowed to dry in air for at least 30 min.

A plasticized PVC membrane was deposited onto the POT coated electrode by drop casting a 60 μL solution of PVC (32.3 wt %), DOS (64.7 wt %), KTFPB (2.4 wt %), and TDMACl

dx.doi.org/10.1021/ac4024999 | Anal. Chem. 2013, 85, 10495−10502

(0.6 wt %) in THF (5% w/v) and was allowed to dry for several hours in air. Oxidation of the POT SC was undertaken using chronoamperometry of the resultant SC ISE in an aqueous solution of 0.1 M NaCl. The electrode potential was held at 1.3 V vs Ag/AgCl (0.1 M NaCl) reference electrode for 20 min to allow adequate time for oxidation of POT with the concomitant permeation of tetrakis[3,5-bis(triflouromethyl)phenyl]borate ($TFPB^-$) into the POT SC. After oxidation of the SC, the PVC membrane was removed by immersing the electrode several times in THF (with a nanoscaled spin-cast film) or by peeling the PVC film from the POT SC (with a microscaled drop cast film), thereby exposing the buried interface of POT SC. Cyclic voltammetry (CV) and chronoamperometric studies were carried out with a Metrohm Autolab-PGSTAT128N using a Ag/AgCl (0.1 M NaCl) reference electrode. All electrochemical impedance spectroscopic (EIS) measurements were performed using a Princeton Applied Research PARSTAT 2263 portable potentiostat. EIS data were collected in the frequency range of 10 mHz to 100 kHz using an excitation potential of 10 mV rms.

SR-XPS and NEXAFS. SR-XPS measurements were carried out on the soft X-ray spectroscopy beamline (14ID) of the Australian Synchrotron, Melbourne, Australia. The insertion device for the beamline is an elliptically polarized undulator providing a flux between 5×10^{11} and 3×10^{12} photons/s/200 mA at the sample at 400 eV. This beamline's optimal energy ranges from 90 to 2000 eV with a resolution ($\Delta E/E$) between 5000 and 10 000 and a beam size of 0.6 mm × 0.6 mm. The data acquisition software used in this study was SPECSlab2. The end-station was constructed by OmniVac and PreVac using a SPECS Phobios 150 hemispherical electron energy analyzer in conjunction with photodiode and drain current detectors. An OmniVac UHV-compatible retarding grid analyzer operating in the partial electron yield mode was utilized for the acquisition of NEXAFS spectra. The vacuum of the analysis chamber was maintained at 2×10^{-10} Torr or better, and the storage ring was operated in the decay mode.

SR-XPS was used to measure the F(1s), C(1s), S(2p), and Au(4f) core orbital binding energies of the control and oxidized SCs. All XPS analysis was performed using a photon energy of 800 eV [as close as practicable to the F(1s) adsorption edge, so as to boost the photoabsorption cross-section and concomitant detection limit for F(1s)] and a pass energy of 10 eV, enabling detection of the weak F(1s) signal originating from the ion-to-electron transduction reaction at the buried interface. All core level binding energies were calibrated against the C(1s) peak from adventitious hydrocarbons (284.6 eV). The POT SC was depth profiled by conducting SR-XPS and NEXAFS analyses at different argon ion sputtering times. The sputtering rate (1.4 nm min^{-1}) was determined by calibrating the ion gun against a POT SC of known thickness, as determined by atomic force microscopy. Depth profiling was continued until the maximum intensity of Au(4f) [originating from the Au(111) substrate] coincided with an absence of S(2p) signal from the POT SC.

EIS/NR. All EIS/NR measurements were undertaken at the 20 MW OPAL research reactor at the Australian Nuclear Science and Technology Organization (ANSTO). NR measurements were recorded using the Platypus time-of-flight neutron reflectometer,[23] employing a cold neutron spectrum (3.0 Å $\leq \lambda \leq$ 18.0 Å) with 23 Hz neutron pulses that had been generated using a disk chopper system (EADS Astrium GmbH) at medium resolution ($\Delta\lambda/\lambda$ = 4%). The reflected neutron beam was recorded on a 2-dimensional helium-3 neutron detector (Denex GmbH) at 0.5° for 30 min and 2° for 2.5 h. The vertical slits were configured for each measurement to maintain a constant beam footprint (7 cm × 3.5 cm), and direct beam measurements were collected under the same collimation conditions for each measured angle. Data reduction and analysis of the neutron reflectivity profiles were calculated using the Motofit reflectometry analysis program.[24]

The NR/electrochemistry measurements were performed in a specially designed electrochemical cell described elsewhere.[25] Silicon wafers were cleaned and prepared using piranha etching and spin coating of polymer films, as described previously.[8] The wafer was immediately spin-coated at 2000 rpm with a 0.3% w/v solution of POT, which was later annealed in a vacuum oven for 3 h at 80 °C. In total, two spin coatings of POT were deemed necessary to achieve a desirable thickness. A plasticized PVC cocktail comprising PVC (32.5 wt %), DOS (65.9 wt %), calcium ionophore IV (1 wt %), and NaTFPB (0.6 wt %) in DMF (1.5% w/v) was subsequently coated onto the SC at a spin rate of 3500 rpm for 1 min. NR and EIS were initially carried out on the POT/PVC ISE in a D_2O electrolyte (0.1 M $CaCl_2$) until no significant changes were observed between successive spectra; i.e., the polymeric ISE had equilibrated with the D_2O electrolyte. The same measurements were also carried out after oxidizing the POT layer at 1.3 V vs the Ag/AgCl (0.1 M $CaCl_2$) reference electrode for 1 h.

RESULTS AND DISCUSSION

The F(1s) core level spectrum (Figure 1a) showed a distinct peak associated with $TFPB^-$ of the POT SC following oxidation of the SC ISE with subsequent removal of the ISE membrane, and this F(1s) signal diminished almost completely after argon ion milling or depth profiling of the POT SC layer. The intensity of the F(1s) peak falls to background levels after only 1 min of argon ion milling or depth profiling, which corresponds to a depth of 14 Å. These results show that $TFPB^-$ was incorporated from the ISE film onto the surface of the POT SC during oxidation but could not be transferred through the POT inferring that the oxidation of POT and concomitant incorporation of $TFPB^-$ is a surface confined process. However, it is important to confirm that this F(1s) signal resulted from migration of $TFPB^-$ during electrochemical oxidation of POT rather than from residual quantities of ISE membrane constituents (peeled from the POT prior to SR-XPS analysis) that may have contaminated the surface of the SC. The former was justified by the absence of Cl(2p) from PVC in the XPS survey scans of all SCs after removing the PVC membrane and rinsing with THF, thereby confirming that the overlayer of ISE was completely removed after peeling of the membrane, which was further confirmed in a quartz crystal microbalance study of the POT layer, where no species were found to dissolve from the underlying POT film even after prolonged exposure to THF.

The S(2p) core level spectra presented in Figure 1b are internally consistent with oxidation of the POT SC and a concomitant incorporation of the $TFPB^-$ species. At the surface prior to sample sputtering, a broad S(2p) core level peak was observed, which is a convolution of two partially offset spin–orbit split doublets [$S(2p_{1/2})$ and $S(2p_{3/2})$] for the oxidized and neutral chemical states of sulfur in POT. While it is expected that the $S(2p_{3/2})$ peak for a neutral thiophene unit should occur at a binding energy of about 163.6 eV, a component exhibiting a slight positive chemical shift (≤1 eV) in the $S(2p_{3/2})$ demonstrates that some of the sulfur exists in an oxidized

dx.doi.org/10.1021/ac4024999 | Anal. Chem. 2013, 85, 10495−10502

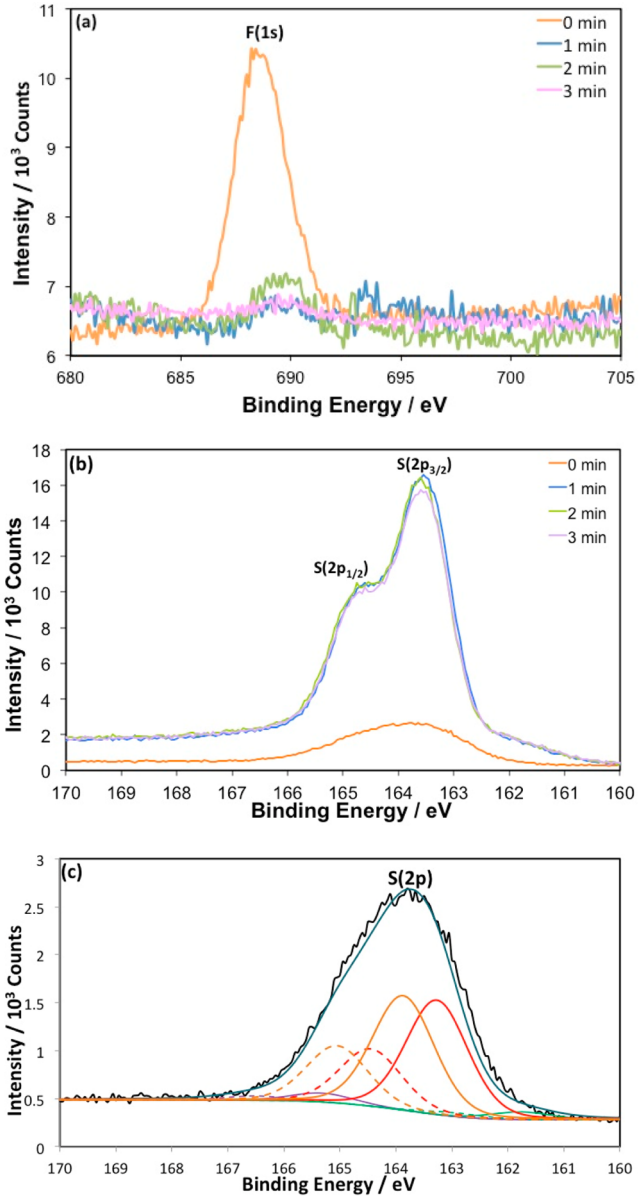

Figure 1. SR-XPS spectra at different sputtering times for an oxidized POT SC, viz., (a) F(1s) core level at 0, 1, 2, and 3 min of Ar ion sputtering, (b) S(2p) core level also at 0, 1, 2, and 3 min Ar ion sputtering, and (c) curve fitted S(2p) core level spectrum of the oxidized POT surface (0 min of sputtering) showing a pair of doublets associated with two chemical forms of sulfur. All binding energies were calibrated against the C(1s) peak from graphitic-like carbon at 284.6 eV.

chemical state (see the curve fitted spectra in Figure 1c). These mixed sulfur oxidation states infer that electrochemical oxidation of a portion of the thiophene units has occurred with a concomitant ingression of the $TFPB^-$ anion.[26] Nevertheless, it is evident that sulfur in thiophene has not been overoxidized to sulfone or sulfate species since the chemical shift for these species would be very high (i.e., 168–169 eV) as compared to the neutral S(2p) peak.[21,27,28] Accordingly, the oxidized form of sulfur is the positively charged thiophene group, or polaron, associated with $TFPB^-$. After only 1 min of sputtering, two partially resolved peaks are observed at binding energies of 163.6 and 165 eV, which are indicative of the $S(2p_{3/2})$ and $S(2p_{1/2})$ spin–orbit split components in neutral sulfur of the POT substrate.[26,29] Furthermore, the low S(2p) intensity of the oxidized POT surface is attributable to the high surface concentration of $TFPB^-$, which creates an overlayer on the surface of the oxidized SC, thereby attenuating the S(2p) photoelectrons emanating from the underlying substrate.

Figure 2a,b presents C(1s) spectra for the oxidized POT SC after 0 and 1 min of Ar ion sputtering, respectively. The

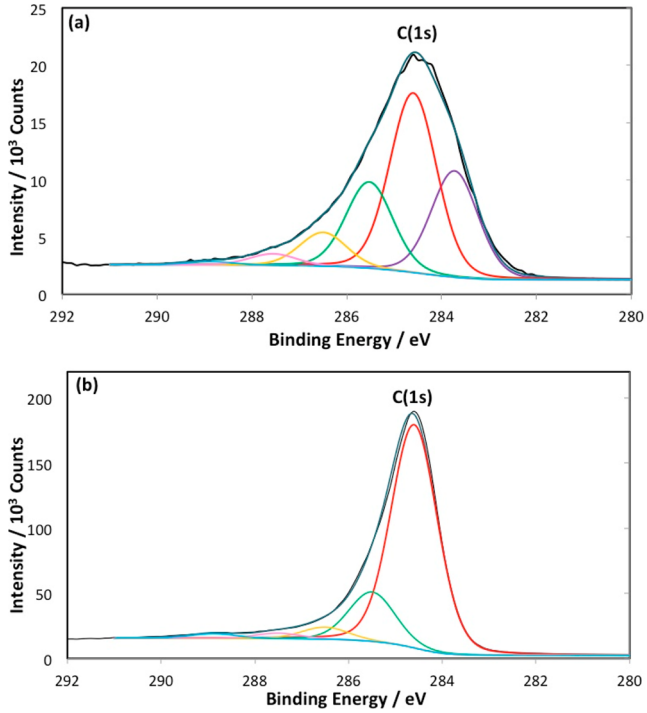

Figure 2. Curve fitted C(1s) spectra for the POT SC at different sputtering times, viz., (a) 0 min of Ar ion sputtering and (b) 1 min of Ar ion sputtering.

oxidized surface (Figure 2a at 0 min of sputtering) gave a major peak at 284.6 eV, which is ascribable to C–C and C=C in POT and $TFPB^-$, while the low binding energy shoulder at 283.7 eV is symbolic of C–B in $TFPB^-$, noting that C carries a partial negative charge.[30] The peaks at about 286 and 287 eV are attributable to C–S and C=S from POT[21] and the peak at approximately 289 eV due to C–F in $TFPB^-$.[31] After 1 min of Ar ion sputtering (see Figure 2b), the C(1s) spectrum only comprised the graphitic-like carbon and C–S and C=S in POT[21] as well as close to background signals for the C–F in $TFPB^-$ peak. Accordingly, the SR-XPS C(1s) spectra are also consistent with a surface confined ionic transference of $TFPB^-$ from the ISE membrane to the oxidized POT SC surface.

NEXAFS studies of the S(2p) absorption edge also suggest that ion-to-electron transduction at the POT SC/ion-selective membrane interface is a surface confined process. The spectra presented in Figure 3 show distinct differences between the sample measured before and after sputtering. Importantly, the fact that excitations arise from two initial states separated by approximately 1 eV (i.e., $2p_{1/2}$ and $2p_{3/2}$) makes it somewhat difficult to interpret the sulfur edge since one essentially has two spectra superimposed and shifted by 1 eV.[30] Nevertheless, the NEXAFS spectra are comparable to those obtained elsewhere for the S(2p) absorption edge of thiophene functional groups.[22,32] The characteristic multiplet peak in the

dx.doi.org/10.1021/ac4024999 | Anal. Chem. 2013, 85, 10495–10502

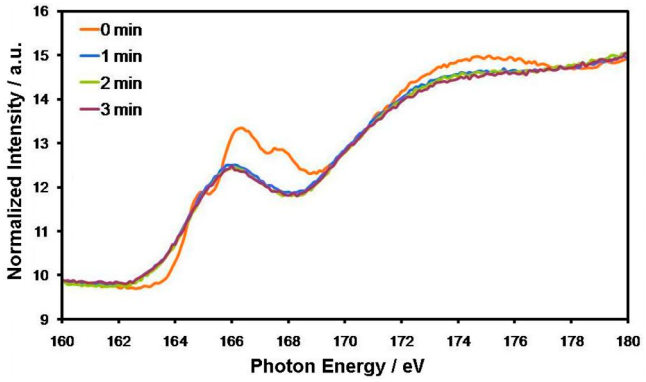

Figure 3. NEXAFS spectra corresponding to the S(2p) core atomic orbital for the POT SC film at 0, 1, and 3 min of Ar ion sputtering.

spectrum obtained prior to sputtering is indicative of a highly oriented chemical species.[22,33] Conversely, the spectra obtained following argon ion sputtering reveals a broad peak, which is suggestive of highly disordered thiophene species, probably randomly orientated polymer molecules in a multitude of chemical states.[34,35] This is not unexpected since sulfur in POT is known to exist in a variety of dispersed chemical states,[36] which would cause considerable overlap in the NEXAFS spectra. The net result of this would be a broad, convoluted peak as seen in the spectrum relating to the bulk of the polymer. The fact that the initial layer (i.e., prior to sputtering) is well-defined provides further credence for the fact that the surface layer has been oxidized into an ordered and highly orientated (virtually crystalline) POT^+TFPB^- species.

In situ EIS/NR was carried out on the POT SC ISE before and after electrochemical oxidation of the POT SC. This provided a robust in situ method for characterization of ion-to-electron transduction, thereby providing a reliable method for corroboration of the ex situ SR-XPS and NEXAFS results. Figure 4 presents NR reflectivity data before and after oxidation of the POT SC also including a theoretical model for a 2-layer system of PVC and POT (see the top right inset graph of neutron scattering length density, ρ, against thickness, z). The NR modeled data shows that the thicknesses of the POT and PVC layers are 48 and 246 Å, respectively, with neutron scattering length densities (SLD) of 2.87×10^{-6} and 0.56×10^{-6} $Å^{-2}$, respectively. Oxidation of the underlying POT SC is confirmed through the Bode phase and complex-plane impedance plots presented in Figure 5a,b, respectively, which show a significant difference in the EIS data during equilibration of the ISE with D_2O compared to that measured after oxidation of the POT SC. This difference (a broadening of the time constant around 1000 Hz) in the Bode phase plot (see Figure 5a), as well as the increase in the resistance of the membrane/POT SC (see the partially resolved semicircle in the expanded inset plot of the high frequency part of the complex-plane impedance plot in Figure 5b), against the conditioned membrane displaying the gradual and usual increase in membrane resistance during equilibration with water,[5,8] is indicative of a new time constant, probably due to the resistance-capacitance coupling of the POT^+TFPB^- surface layer formed via oxidation of POT. In contrast, there is no evidence for oxidation of the POT SC in the NR data. Importantly, an attempt to fit a theoretical model directly to the oxidized POT based on such small differences in neutron reflectivity would not be a statistically valid scenario. Instead, we have developed and presented two theoretical models based on the initial parameters of the fitted model of the neutral POT, as illustrated in Figure 4, and also included in Figure 6 for comparative purposes. The other models pertain to two extreme cases, which may occur during the electrochemical oxidation of the POT SC, namely, a surface confined oxidation reaction and complete oxidation of the SC film. In the former model, we have assumed a neutral POT thickness of 34 Å and an oxidized POT (i.e., POT^+TFPB^-) overlayer of 14 Å in thickness, providing a NR pattern closely resembling the neutron reflectivity data for electrochemically oxidized POT SC (compare Figures 4 and 6). On the other hand, the theoretical model for completely oxidized POT (all 48 Å of POT was converted into POT^+TFPB^-) bears almost no resemblance to the initial neutral POT model or the actual data set for the oxidized POT SC system. These outcomes provide convincing indirect evidence for a surface confined oxidation of POT.

The results of this study strongly support the thesis that ion-to-electron transfer at the PVC/POT SC buried interface involving the bulky $TFPB^-$ anion is a surface confined reaction. It is important to note that Ivaska and co-workers[37,38] utilized EIS to demonstrate that smaller and more mobile anions such as BF_4^- and ClO_4^- are capable of penetrating the bulk of oxidized POT films, as inferred by a massive increase in film conductivity following oxidation and concomitant anion incorporation into the POT film together with the low anion diffusion coefficients that are internally consistent with diffusion in the solid state. Also, electron spin resonance (ESR) has shown that POT oxidation and anion incorporation with small anions occurs in the bulk of the electropolymerized POT.[39]

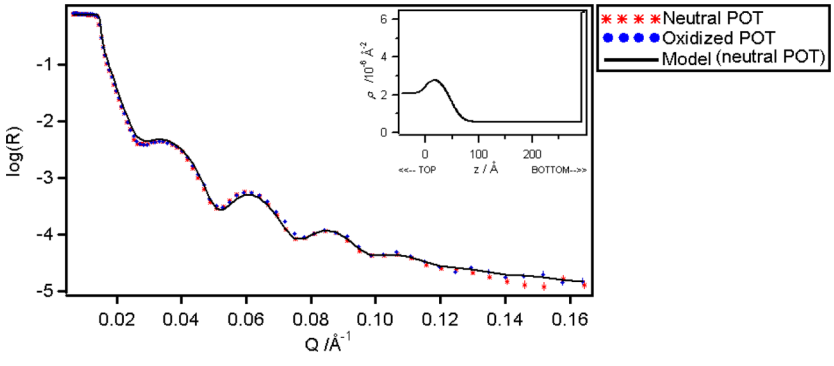

Figure 4. NR spectra of a POT SC prior to and after electrochemical doping with $TFPB^-$. The modeled fit is also included for the neutral POT. The inset pertains to the scattering length density profile of the neutral POT model.

dx.doi.org/10.1021/ac4024999 | Anal. Chem. 2013, 85, 10495−10502

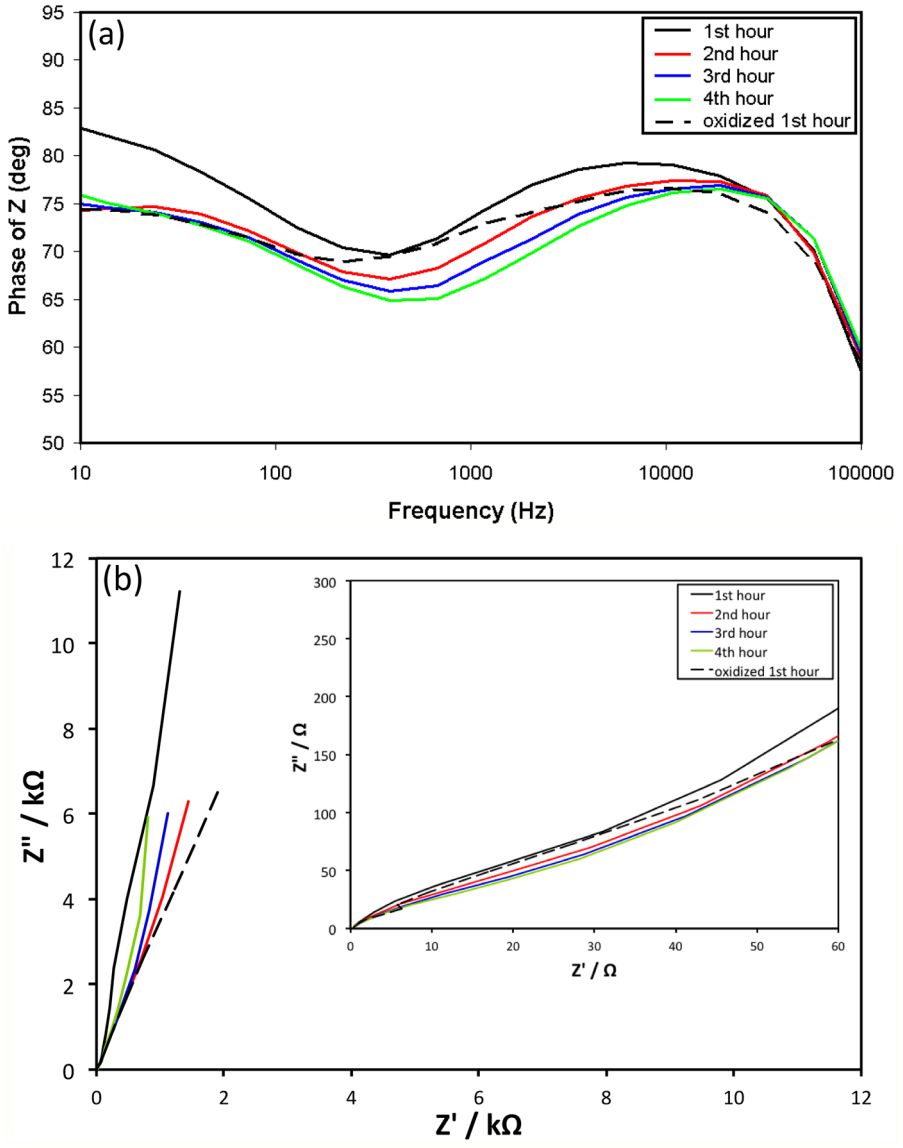

Figure 5. (a) Bode phase plots and (b) complex-plane plots for the SC ISE system while bathing in a D_2O electrolyte and also after electrochemical oxidation of POT with a concomitant exchange of $TFPB^-$ at the buried interface.

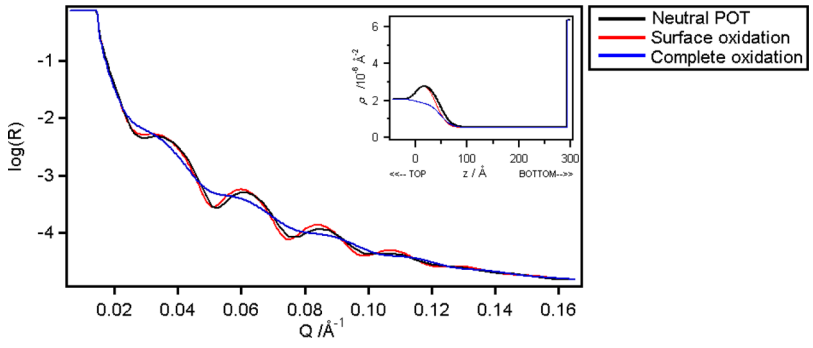

Figure 6. Theoretical NR models for the surface confined oxidation of POT and complete oxidation of the POT SC layer. These models are based on the parameters obtained for neutral POT, as shown in Figure 4. The inset presents the neutron scattering length density profile for the three theoretical models.

Accordingly, this slow diffusion rate of $TFPB^-$ in the solid-state POT material is expected to limit the ion-to-electron transduction reaction to the surface of POT. The chronoamperogram obtained from the oxidation of the POT SC revealed that the electrochemical reaction was instantaneous and completed within 2 min. Nevertheless, the oxidation potential was held for a further 18 min in the SR-XPS experiment and a further 58 min in the NR experiment to allow adequate time for

dx.doi.org/10.1021/ac4024999 | *Anal. Chem.* 2013, 85, 10495−10502

oxidation of POT and transgression of $TFPB^-$ into the POT. Since both experimental results confirmed a surface confined reaction, it is obvious that the timeframes of the experiments were not a limitation to the ion-to-electron transduction reaction in POT.

Importantly, this new knowledge about surface confinement of charge-transfer events at the buried interface of the electropolymerized POT SC ISE has important ramifications for the electrochemical sensor community. It is obvious that a thicker layer of the POT conductive polymer is not necessary for SC fabrication, noting that Angstrom or micrometer thick layers are equally capable of eliminating undesirable water layers in POT SC ISEs.[8] A surface confined spontaneous oxidation of the POT layer leads to the establishment of a mixed redox state of the CP (oxidized overlayer of CP on top of unoxidized CP). A mixed redox state is expected to give rise to a well-defined and stable interfacial potential due to the high redox buffering ability of these surface states. Consequently, this explains why the electropolymerized POT SC ISE based on this ion-to-electron transducer give rise to stable potential readings.

Since only a monolayer of electropolymerized POT SC material actively acts as ion-to-electron transducer, it may also explain why SAM SC systems[7,10−14] have been utilized successfully as SC ISEs. The POT SC surface confined ion-to-electron transduction reaction mechanism may equally explain why other SCs such as three dimensionally ordered macroporous carbon[15] and single-walled carbon nanotubes[16,17] are also capable of functioning effectively as SC ISEs. Since the charge-transfer reaction need only take place at the SC surface, one expects that the ion-to-electron transduction process is associated with a high double layer capacitance. It has been established that SC materials possessing a high double layer capacitance, such as single-walled carbon nanotubes and three dimensionally ordered macroporous carbon,[15,16] are capable of functioning effectively as SCs. This new information may motivate sensor researchers with the development of new redox active or capacitive SC materials for ISEs.

CONCLUSIONS

The results of this study demonstrate unequivocally that ion-to-electron transduction in the electropolymerized POT SC ISE occurs via a surface confined charge-transfer reaction coupled with ion transfer across the ISE membrane/SC interface. It was found that, after oxidation of the POT SC even for 1 h at high anodic potentials, $TFPB^-$ and POT^+ were confined to the outer surface of the POT SC; they did not penetrate the bulk of the POT layer. SR-XPS and NEXAFS spectra of fluorine, carbon, and sulfur after sputtering of the oxidized POT layer to a depth of 14 Å were consistent with unoxidized POT not containing any $TFPB^-$, thereby confirming restriction of ion-to-electron transduction to the surface layer of the POT SC. These outcomes were further substantiated by EIS measurements and modeling of NR data for two extreme-case scenarios (i.e., a surface confined oxidation and complete oxidation of the POT SC film). Theoretical modeling of a surface confined ion-to-electron transduction process closely matched the experimental NR data for the electrochemically oxidized POT SC. These outcomes have important ramifications for the sensor research community as they provide new insights into the reaction mechanism of ion-to-electron transduction in the POT SC ISE, with the performance of the electropolymerized POT SC not depending on the thickness or extent of ion diffusion within the electropolymerized material. This results in a POT SC that naturally exists in a mixed oxidation state, which for the first time offers a plausible explanation for the high stability of potential readings of this SC material. On the basis of the results reported in this work, it appears necessary to only utilize a molecularly thin layer of the electropolymerized POT SC (below the penetration depth of the counterion) for optimal performance of the SC ISE.

AUTHOR INFORMATION

Corresponding Author

*E-mail: rdemarc1@usc.edu.au. Tel: +61 7 5430 2867. Fax: +61 7 5456 5544.

Notes

The authors declare no competing financial interest.

ACKNOWLEDGMENTS

Financial support from the Australian Research Council (Projects LX0776015 and DP0987851) is gratefully acknowledged. One of us (J.-P.V.) thanks the Australian Institute of Science and Engineering (AINSE) for a Postgraduate Research Award. Part of this work was undertaken on the soft X-ray spectroscopy beamline at the Australian Synchrotron (AS), Victoria, Australia. We are very grateful to Dr. Bruce Cowie and Dr. Anton Tadich at the AS for assistance and advice in the running and interpretation of SR-XPS and NEXAFS spectra. Eric Bakker acknowledges support from the Swiss National Science Foundation for this research.

REFERENCES

(1) Cattrall, R. W.; Freiser, H. *Anal. Chem.* **1971**, *43*, 1905−1906.
(2) Cattrall, R. W.; Drew, D. M.; Hamilton, I. C. *Anal. Chim. Acta* **1975**, *76*, 269−277.
(3) Hauser, P. C.; Chiang, D. W. L.; Wright, G. A. *Anal. Chim. Acta* **1995**, *302*, 241−248.
(4) Bobacka, J. *Anal. Chem.* **1999**, *71*, 4932−4937.
(5) De Marco, R.; Veder, J. P.; Clarke, G.; Nelson, A.; Prince, K.; Pretsch, E.; Bakker, E. *Phys. Chem. Chem. Phys.* **2008**, *10*, 73−76.
(6) Sutter, J.; Radu, A.; Peper, S.; Bakker, E.; Pretsch, E. *Anal. Chim. Acta* **2004**, *523*, 53−59.
(7) Fibbioli, M.; Bandyopadhyay, K.; Liu, S.-G.; Echegoyen, L.; Enger, O.; Diederich, F.; Gingery, D.; Buhlmann, P.; Persson, H.; Suter, U. W.; Pretsch, E. *Chem. Mater.* **2002**, *14*, 1721−1729.
(8) Veder, J. P.; De Marco, R.; Clarke, G.; Chester, R.; Nelson, A.; Prince, K.; Pretsch, E.; Bakker, E. *Anal. Chem.* **2008**, *80*, 6731−6740.
(9) Bobacka, J.; Ivaska, A.; Lewenstam, A. *Chem. Rev.* **2008**, *108*, 329−351.
(10) Grygolowicz-Pawlak, E.; Wygladacz, K.; Sek, S.; Bilewicz, R.; Brzozka, Z.; Malinowska, E. *Sens. Actuators, B* **2005**, *111−112*, 310−316.
(11) Grygolowicz-Pawlak, E.; Plachecka, K.; Zbigniew, B.; Malinowska, E. *Sens. Actuators, B* **2007**, *123*, 480−487.
(12) Fibbioli, M.; Enger, O.; Diederich, F.; Pretsch, E.; Bandyopadhyay, K.; Liu, S.-G.; Echegoyen, L.; Buhlmann, P. *Chem. Commun.* **2000**, *5*, 339−340.
(13) Sek, S.; Bilewicz, R.; Grygolowicz-Pawlak, E.; Grudzien, I.; Brzozka, Z.; Malinowska, E. *Pol. J. Chem.* **2004**, *78*, 1655−1665.
(14) Grygolowicz-Pawlak, E.; Palys, B.; Biesiada, K.; Olszyna, A. R.; Malinowska, E. *Anal. Chim. Acta* **2008**, *625*, 137−144.
(15) Lai, C.-Z.; Fierke, M. A.; Stein, A.; Buehlmann, P. *Anal. Chem.* **2007**, *79*, 4621−4626.
(16) Crespo, G. A.; Macho, S.; Bobacka, J.; Rius, F. X. *Anal. Chem.* **2009**, *81*, 676−681.
(17) Crespo, G. A.; Macho, S.; Rius, F. X. *Anal. Chem.* **2008**, *80*, 1316−1322.
(18) Kim, Y.; Amemiya, S. *Anal. Chem.* **2008**, *80*, 6056−6065.

(19) Si, P.; Bakker, E. *Chem. Commun.* **2009**, *35*, 5260−5262.
(20) Chumbimuni-Torres, K. Y.; Rubinova, N.; Radu, A.; Kubota, L. T.; Bakker, E. *Anal. Chem.* **2006**, *78*, 1318−1322.
(21) De Marco, R.; Jee, E.; Prince, K.; Pretsch, E.; Bakker, E. *J. Solid State Electrochem.* **2008**, *13*, 137−148.
(22) Hitchcock, A. P.; Horsley, J. A.; Stohr, J. *J. Chem. Phys.* **1986**, *85*, 4835−4848.
(23) James, M.; Nelson, A.; Holt, S. A.; Saerbeck, T.; Hamilton, W. A.; Klose, F. *Nucl. Instrum. Methods Phys. Res., Sect. A* **2011**, *632*, 112−123.
(24) Nelson, A. *J. Appl. Crystallogr.* **2006**, *39*, 273−276.
(25) Veder, J. P.; De Marco, R.; Clarke, G.; Jiang, S. P.; Prince, K.; Pretsch, E.; Bakker, E. *Analyst* **2011**, *136*, 3252−3258.
(26) Kang, E. T.; Neoh, K. G.; Tan, K. L. *Phys. Rev. B* **1991**, *44*, 10461−10469.
(27) Kang, E. T.; Neoh, K. G.; Tan, K. L. *Macromolecules* **1992**, *25*, 6842−6848.
(28) Kaul, A.; Udipi, K. *Macromolecules* **1989**, *22*, 1201−1207.
(29) Riga, J.; Snauwaert, A.; De Pryck, R.; Lazzaroni, R.; Boutique, J. P.; Verbist, J. J.; Bredas, J. L.; Andre, J. M.; Taliani, C. *Synth. Met.* **1987**, *21*, 223−228.
(30) Il'inchik, E. A. *J. Appl. Spectrosc.* **2008**, *75*, 883−891.
(31) Moulder, J. F.; Stickle, W. F.; Sobol, P. E.; Bomben, K. D. *Handbook of X-ray photoelectron spectroscopy*; Perkin-Elmer Corporation: Eden Prairie, Minnesota, 1992.
(32) Tourillon, G.; Mahatsekake, C.; Andrieu, C.; Williams, G. P.; Garret, R. F.; Braun, W. *Surf. Sci.* **1988**, *201*, 171−184.
(33) Okajima, T.; Narioka, S.; Tanimura, S.; Hamano, K.; Kurata, T.; Uehara, Y.; Araki, T.; Ishii, H.; Ouchi, Y.; Seki, K.; Ogama, T.; Koezuka, H. *J. Electron. Spectrosc. Relat. Phenom.* **1996**, *78*, 379−382.
(34) Dubey, M.; Weidner, T.; Gamble, L. J.; Castner, D. G. *Langmuir* **2010**, *26*, 14747−14754.
(35) Kobayashi, E.; Okudaira, K. K.; Okajima, T. *Surf. Interface Anal.* **2012**, *44*, 740−743.
(36) Riga, J.; Snauwaert, P.; De Pryck, A.; Lazzaroni, R.; Boutique, J. P.; Verbist, J. J.; Brédas, J. L.; André, J. M.; Taliani, C. *Synth. Met.* **1987**, *21*, 223−228.
(37) Bobacka, J.; Ivaska, I.; Grzeszczuk, M. *Synth. Met.* **1991**, *44*, 9−19.
(38) Bobacka, J.; Ivaska, I.; Grzeszczuk, M. *Synth. Met.* **1991**, *44*, 21−34.
(39) Albery, W. J.; Chen, Z.; Horrocks, B. R.; Mount, A. R.; Wilson, P. J.; Bloor, D.; Monkman, A. T.; Elliott, C. M. *Faraday Discuss. Chem. Soc.* **1989**, *88*, 247−259.